IJCRT.ORG ISSN : 2320-2882

INTERNATIONAL JOURNAL OF CREATIVE RESEARCH THOUGHTS (IJCRT)

An International Open Access, Peer-reviewed, Refereed Journal

GRAPHENE BASE BIOMEDICAL TECHNOLOGY

Tarun Radadiya

PG Data Science Student of Amity University (India), Data Analyst Student of eCornell University (USA), Team Lead in Paytm

Abstract:-Graphene a single layer 2-dimensional structure nano material with unique physicochemical properties (e.g. high surface area, excellent electrical conductivity, strong mechanical strength, unparalleled thermal conductivity, electrochemical, remarkable biocompatibility and ease of functionalization), has received increasing attention in physical, chemical and biomedical fields. Single-layer graphene oxide sheets down to a few nanometers in lateral width. We develop functionalization chemistry to impart solubility and compatibility of GO in biological environments. Graphene based materials for biomedical applications. In particular, graphene based biosensors for small biomolecules (glucose, dopamine etc.), proteins and DNA detection have been summarized graphene based bioimaging, drug delivery, photo thermal therapy, biosensor , gene delivery , tissue engineering , cell growth , steam cell differentiation, cancer treatment ,mass spectrometry application of graphene use in biomedical.

Keyword: **Graphene, Graphene oxide, Graphene properties, Biomedical application.**

I. INTRODUCTION

Graphene, a single-atom-thick layer of sp2 hybridized carbon atoms arranged in a honeycomb lattice, is the basic building block of other carbon allotropes including 0D fullerenes, 1D carbon Nanotube, and 3D graphite [1]. New graphene based materials have been making a profound impact in energy technology [2–4], sensors [5–7], catalysis [8], and bioscience/biotechnologies [9–11] due to their unique physicochemical properties. These include high surface area (2630 m2/g) [12], excellent electrical conductivity (1738 siemens/m) [13], strong mechanical strength (about 1100 GPa) [14], unparalleled thermal conductivity (5000 W/m/K) [15], and ease of functionalization [16,17]. Graphene based materials demonstrate excellent electrochemical and optical properties, as well as the capability to adsorb a variety of aromatic biomolecules through a p–p stacking interaction and/or electrostatic interaction, which make them ideal materials for constructing biosensors and loading drugs. Moreover, thanks to abundant oxygen-containing groups attached to its honeycomb like sixatom carbon rings, graphene oxide (GO) (as one of the raw materials) can be readily modified with targeting ligands to facilitate targeted imaging and drug delivery [18]. Since the first application for drug delivery was reported by Dai et al. [11,19], graphene based materials have been intensively investigated in the area of biomedicine and show promising potential in this Field [20–22].

Graphene, a two-dimensional carbon sheet with single atom thickness has recently received significant interest due to its unique mechanical and electrical properties. Graphene is grown via chemical vapor deposition from carbon-containing gases on the surface of catalytic metals including Co, Pt, Pd, Ni, and Fe [28]. Graphene derivatives possess high biocompatibility, physiological solubility and stability which make it efficient for biomedical applications such as bioimaging, drug delivery, photo thermal therapy, biosensor, gene delivery, tissue engineering, cell growth, steam cell differentiation, cancer treatment, mass spectrometry and biocompatible scaffold for
Cell culture (Figure 1).

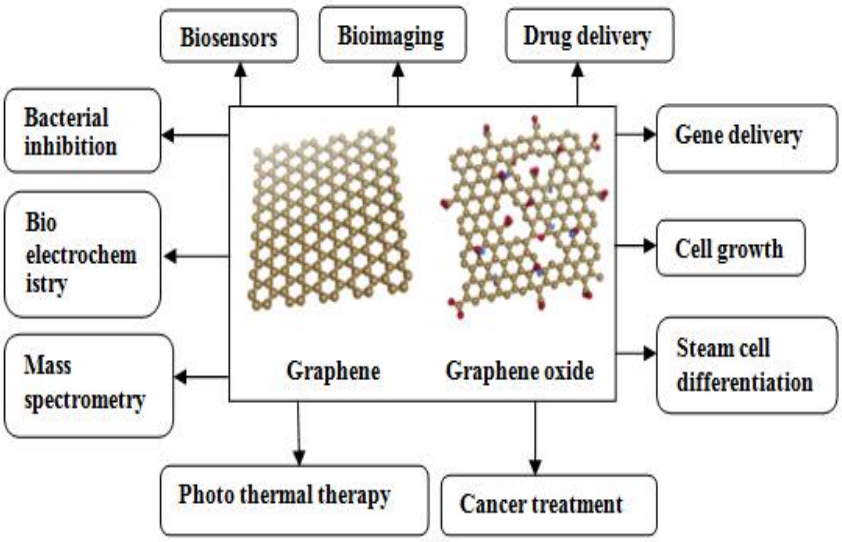

Figure:-1 Graphene application in biomedical

These applications utilized the properties of graphene in different ways. For example, graphene demonstrates advantageous characteristics for use in electrochemical and optical biosensors thanks to its unique electrical and optical properties [23]. Utilizing its large surface area and sp2-bonded carbon atoms, graphene has been widely used to selectively enrich and detect aromatic molecules and single-stranded DNA (ssDNA) through p–p stacking interactions [11,19,24]. Graphene oxide is very easily functionalized thanks to its abundant oxygencontaining groups [25]. GO has also been used as a photothermal agent for cancer treatment with encouraging therapeutic outcomes due to its high, intrinsic near-infrared (NIR) absorbance [26, 27].

II. BIOSENSOR

Graphene oxide (GO), an amorphous insulator material, has consists of a hexagonal ring based carbon network having both sp2-hybridized carbon atoms and sp3-hybridizedcarbons bearing hydroxyl andep oxide functional groups on either side of the sheet, whereas the sheet edges are mostly decorated by carboxyl and carbonyl groups [29-34]. These unique properties hold great promise for potential applications in many technological aspects such as nanoelectronics [35-38], nanophotonics [39-44], and bio-sensors [37, 45-49], and nanocomposites [50, 51].

The introduced a novel and simple methods for fabricating high-sensitivity, high-resolution GO based SPR biosensors that provide high accuracy and precision over relevant ranges of analyte measurement. We used SPR technique to detect the binding phenomenon between proteins and GO films. SPR is a surface-sensitive optical technique that very suitable for Monitoring of bio-molecular interactions occurring in very close vicinity to sensor surfaces. It allows real-time and label-free detection of analysis by exploiting the interfacial refractive index changes associated with any affinity binding interaction between a biomolecule immobilized on a sensor surface and its biospecific partner in solution. Rapid and real-time analysis without labeling, highly specific detection with extremely low detection limit screating the unique potential for the application of SPR in biosensor. Owing to these powerful advantages of GO-based SPR technique, many applications of GO-based biosensors in such areas as molecular engineering, biomedical diagnostics, drug discovery, environmental monitoring and food analysis [53].

Figure 2(a),(b) shows the design of two sensing chips, i.e., a conventional SPR chip and a GOS film-based SPR chip. Standard SPR thin films were deposited with thin film for gold (Au) thickness of 47 nm and chromium (Cr) thickness of 2 nm on BK7 glass substrate to a thickness of 0.17 mm. SPR experiments were conducted using a BI-3000G SPR system with Kretschmann prism coupling (Biosensing Instrument, Tempe, AZ, USA). The test injection Sample volume was 200 µl and the flow rate was60 µl/s. All experiments were performed at 25°C and repeated in triplicate.

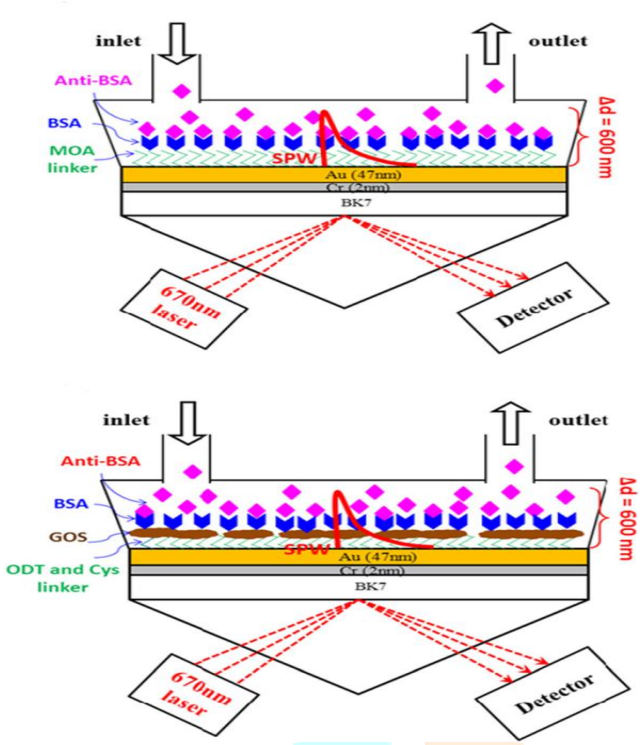

Figure:-2 SPR biosensor chip uses an immunoassay method for detecting a protein using a gold binding. (a) Conventional SPR chip and (b) GOS film-based SPR chip. Intensity of an evanescent field with a depth of approximately 100 ~ 500 nm decays exponentially with increasing distance from the metal

Bimolecular binding, observed within approximately 10 nm of the metal surface, gives rise to a higher signal shift response than that of the interactive process at a distance of 300 nm there from. For typical SPR Kretschmann prism coupling that uses a red light to induce the evanescent field, its field intensity is no more than 600 nm in practice.

Figure 2a presents a conventional SPR sensing chip and a biomolecule binding mechanism. 8-Mercaptooctanoic acid (MOA; Sigma-Aldrich Co. LLC., St. Louis, MO, USA) is activation of carboxylic acid-terminated thiol self assembled monolayers (SAMs) on a modified Au surface.
MOA binds to the Au surface through their thiol linker (−SH end) resulting monolayers, which are terminated with carboxylic acid (−COOH). The MOA can be further functionalized to immobilize a bovine serum albumin (BSA; Sigma, Chemical Company, St. Louis, MO, USA) protein. Anti-BSA protein interactions are performed as well.

Figure 2b shows a GOS film-based SPR chip with its biomolecule binding mechanism. Two binding mechanisms are functionalized SAMs on amino-modified Au surfaces by solutions of cystamine (Cys; Alfa Aesar Co., Ward Hill, MA, USA) with a concentration of 5 mM and octadecanthiols (ODT, C18H37SH; Sigma-Aldrich Co. LLC.) with a concentration of 10 mM formation of Au-S bonds that immobilize a GOS. Concentration of the GOS diluted in water was 2 mg/ml. The GOS film sensing surface detects BSA protein concentrations in a range of 100 pg/ml to 100 µg/ml and their interaction with anti-BSA. Moreover, analysis is performed of the kinetics of protein-protein interactions at physical contacts that are established between two proteins, owing to biochemical events, protein affinity adsorption forces, and protein binding forces [52].

III. FIELD EFFECT TRANSISTOR BIOSENSORS

Field effect transistor (FET) is a voltage controlled device which is capable of varying a current across a semiconducting channel by the application of an electric field. In a graphene field effect transistor (GFET) the graphene sheet acts as the semiconducting channel between two metal source and drain electrodes which lie atop an electrical insulator such as SiO2. When charged biological molecules bind on the surface of the semiconducting graphene sheet in the GFET there is a measureable change in resistance. The GFET device is able to act as a real-time all electronic biosensor based on this detection principle

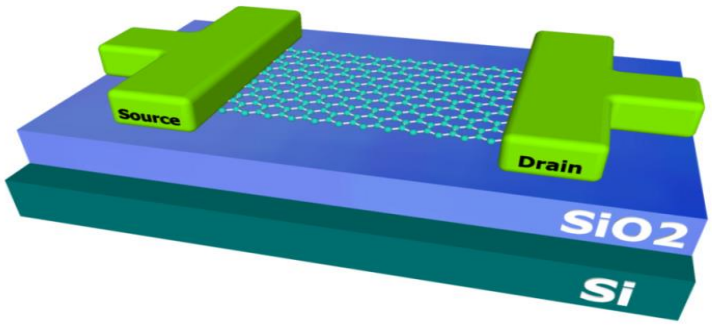

Figure:-3 Graphene field effect transistor.

Successfully used a label free GFET device to detect bovine serum albumin [54], Immunoglobulin E,[67] and show that GFET's have sensitivity under several
Hundred pico moles per liter.[55] This recent work has shown that GFET biosensing devices are promising candidates over CNT devices, however the graphene used in these experiments was obtained through mechanical exfoliation. As discussed previously, this method is not practical for cost and time effective production of a GFET biosensing device.

The need for a cost effective POC graphene based biological sensor will require the use of a GFET device which uses CVD graphene. Several groups are currently experimenting with label free GFETs which incorporate CVD graphene, [65,56,57] and have successfully detected DNA hybridization,[57] glucose oxidase,[56] and glutamic dehydrogenase.23 The detection limits of the glucose and glutamate sensors are comparable to CNT,[58] and graphene based electrochemical biosensors which use methods to obtain graphene other than mechanical exfoliation,[59] however are still inferior to nano wire,[60] and CNT[61] based electrochemical biosensors. The recent attention and work dedicated to the large scale production of high quality graphene will likely show that graphene is a practical and superior alternative to other Nano materials which are incorporated into biosensors.

Thrombin Protein

Thrombin protein is produced by the body and has an important role in the blood clotting or coagulation process,[62] and the regulation of tumor growth.[63] The selective and sensitive detection of thrombin may be useful in surgical procedures and cardiovascular disease therapy.[63] There have been many efforts to produce a sensitive biological sensor for the detection of thrombin.[66,64] In the past, thrombin has been optically detected using a fluorescence based tag,[64] which we have previously discussed as a slow and costly method for detection. In this paper we will address the feasibility of a CVD graphene based label free FET biosensor to accurately detect thrombin.

IV. BIOIMAGING

The Recently fluorescent carbon-based nanomaterials, including carbon dots (C-Dots), graphene oxide (GO) nanoparticles, and the emerging graphene quantum dots (GQDs) are attracting increasing interest in the field of bioimaging for their good biocompatibility and photostability.[67−71]Sun et al. reported the multiphoton imaging of surface-passivated C-Dots with a higher two-photon absorption cross section of 39 000 Göppert-Mayer units (GM).16 The two-photon fluorescence of polyethylene glycol linked GO nanoparticle with a size of ~30 nm was applied to in vitro and in vivo bioimaging,obtaining an imaging depth of 300 μm.[73,74] Two-photon imaging using the GQD has also been reported for cell labeling[75]. The quasi zero-dimensional GQD with a single atomic layer gives rise to several advantages over other carbonbased nanomaterials for potential deep-tissue TPFI. First, the bandgap and fluorescence of GQDs can be effectively tuned by doping hetero atoms to the π-conjugated system [76−80]. A blue shift in fluorescence emission has been reported for GQDs after doped with nitrogen atom through an electrochemical method due to the strong electron-withdrawing effect of the doped nitrogen[76]. It can be expected that doping nitrogen through introducing strong electron-donating groups such as dimethylamido could result in a red shift of fluorescence and achieve longer emission and excitation wavelengths[81],

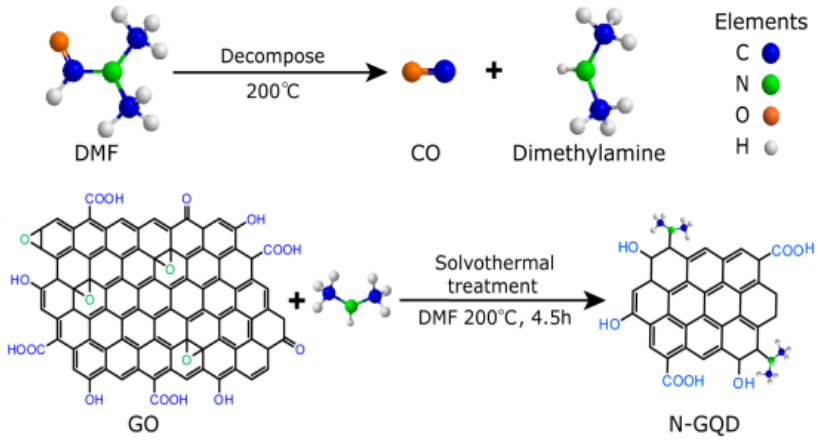

Figure:-4. (a) Decomposition of DMF at a high temperature. (b) Schematic illustration of the strategy for the N-GQD preparation.

which are less scattered by biotissues and more practical for bioimaging. Second, GQDs without passivation by any surfactant can exhibit strong fluorescence induced by a pronounced quantum confinement and edge effect,14[82−84] which could also impart a larger two-photon absorption cross section and deeper penetration in turbid tissues[85-87]. Third, the large rigid π- conjugated electronic structure of GQD can also improve the intra molecular charge transfer efficiency and therefore enhance the two-photon absorption to achieve larger imaging depth in TPFI [88].

To the best of our knowledge, no efforts have focused on the two-photon absorption and fluorescence property of GQD under femtosecond laser excitation, and no research about application of GQD as two-photon fluorescent probe for deep tissue TPFI has been reported so far. In this work, we developed a facile solvothermal approach for doping nitrogen to GQD using dimethylformamide (DMF) as both solvent and nitrogen sources. Two-photon-induced fluorescence of N-GQD was systematically investigated using near-infrared (NIR) femtosecond laser as excitation and applied for efficient twophoton cellular and deep-tissue imaging.

The large imaging depth achieved by N-GQD significantly extends the fundamental two-photon imaging depth limit in scattering tissues. Furthermore, the good biocompatibility and extraordinary photo stability support the potential application of N-GQD in long-term TPFI of biological tissues. The N-GQD was prepared through a facile one-pot solvothermal approach using GO as a precursor. GO was obtained by a modified Hummer's method [89]. This chemically derived GO is a two dimensional network of sp2- and sp3- bonded atoms and shows unique heterogeneous chemical structure in which aromatic sp2 domains are surrounded by sp3- hybridized carbon atoms. The sp2 domains in GO are calculated to have a mean size of 2.7 nm according to the empirical Tuinstra−Koenig relationship [82, 90]. To effectively introduce nitrogen with strong electron-denoting effect into GQD, DMF served as a solvent and source of nitrogen as it could be decomposed to dimethylamine[91] (a strong electron denoting group) and carbon monoxide at temperature higher than its boiling point (Figure 4a). Then the decomposed dimethylamine was doped into the GO to yield 1,2-amino alcohol via nucleophilic ring-opening reaction with the epoxy group on the surface of GO,[82,92] thus enabling the extraction of smaller sp2 domains from the large GO sheet and simultaneous bonding of dimethylamine with the aromatic ring to form NGQD as illustrated in Figure 4b.

N-GQD Preparation

The N-GQD was prepared through a facile one-pot solvothermal method. In brief, the graphene oxide (GO) was dissolved in dimethylformamide (DMF) with a concentration of ~200 mg ml-1. The GO and DMF mixed solution was ultrasonicated for 30 minutes (120 W, 100 kHz) and then transferred to a poly(tetrafluoroethylene)-lined autoclave (30 ml) and heated at 200 °C for 4.5 h. After cooling to room temperature naturally, the obtained mixture was filtered through a 0.22 μm microporous membrane to remove the black precipitates, obtaining a brown solution. The solvent was removed with the aid of a rotary evaporator. Then the obtained N-GQD was dispersed in DI water. In fact, heating DMF at 200 °C for 4.5 h generated a small amount of impurities which could not be totally removed by evaporation. We further found that these DMF residues could emit blue fluorescence under UV lamp irradiation. Therefore,

the obtained N-GQD must be dialyzed through a 500 Da dialyzer for at least 48 hours to totally remove the DMF residues until there was no blue fluorescence detected in the dialysis solution outside the dialyzer bag. Then the obtained pure N-GQD was used for further characterization. The control experiment was also performed in the absence of DMF. GO was dissolved in DI water and applied for hydrothermal process under the same conditions. Under UV irradiation, the obtained GQD without nitrogen doping showed blue fluorescence rather than the green fluorescence of N-GQD. The fluorescence spectrum of GQD aqueous solution showed a maximum fluorescence peak at 450 nm (Ex 390 nm), which was consistent with the reported papers. Compared with GQD, the maximum emission peak shifted to 520 nm for N-GQD (Figure S1) with the same excitation wavelength, indicating the solvothermal process using DMF could successfully realize the nitrogen doping of GO to form the new N-GQD.

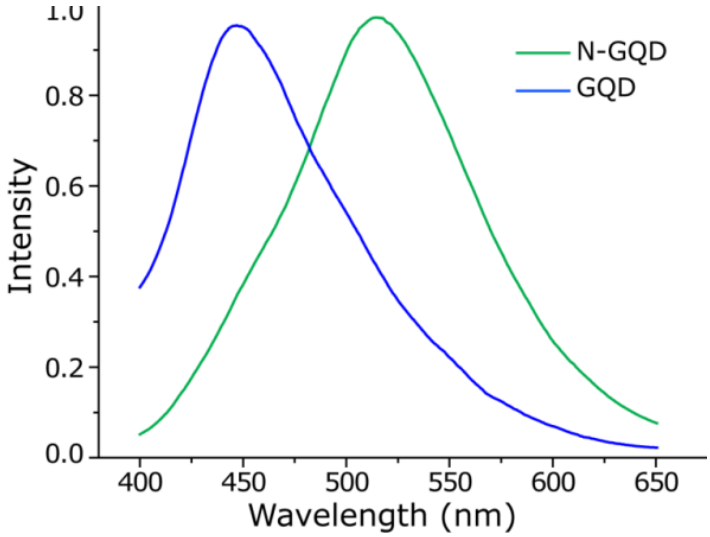

Figure:-5. Fluorescence spectra of GOD (blue line) and N-GQD (green line), ex: 390 nm.

Two-Photon Cellular Imaging

A Nikon Fluoview multiphoton microscope (FV1000MPE) was used for two-photon luminescence imaging of N-GQD and Hela cells. A mode-locked Ti:Sapphire laser (MaiTai, Spectra Physics) with pulses of 100 fs at a repetition rate of 80 MHz was used as the excited light source. For cellular imaging, Hela cells were cultured in high-glucose modified Eagle's medium supplemented with 10% fetal bovine serum and 1% penicillin/streptomycin (HDMEM) using a four-chambered Lab-Tek coverglass system (Nalge Nunc) (approximately 5 × 105 in each well). All cells were incubated at 37 °C in a CO2 incubator until approximately 80% confluence was reached. The aqueous solution of the N-GQD (1 mg ml-1) was filtered through a 0.22 μm membrane (Millipore Express). Then the filtered solution (~50 μl) was mixed with the culture medium (1,000 μl) and added to three wells of the glass slide chamber (the fourth well used as a control) in which the Hela cells were grown. After incubation for 2 h, the Hela cells were washed three times with PBS (500 μl each time) and kept in PBS for two-photon imaging on the FV1000MPE with excitation at 800 nm using a water objective lens (60×). The laser power used for two-photon imaging was measured to be 1mW at the focal plane.

Cytotoxicity Evaluation.

The cells were cultured first for 24 h in an incubator (37 °C, 5% CO2), and for another 24 h after the culture medium was replaced by DMEM high glucose containing the N-GQD at different concentrations (0, 5, 15, 25, 50, 100, 200, 400 μg ml^{-1}). Then, 10 μl CCK-8 reagents mixed with 100 μl DMEM high glucose was added to each cell well. After further incubation for 4 h, the optical density (OD) of the mixture was measured at 450 nm. The cell viability was estimated according to the following equation: Cell Viability [%] = (ODtreated / ODcontrol) × 100% (ODcontrol was obtained in the absence of N-GQD, and ODtreated obtained in the presence of N-GQD.) Each experiment was performed four times and the average data was presented.

Two-Photon Deep-Tissue Imaging

For the 0~800 μm imaging depth, the excitation powers were adjusted so that approximately the same signal-to-noise ratio (SNR) could be achieved at a constant frame rate of 1 fps, starting with 20 mW for the 0 um imaging depth. At the imaging depths beyond 800 μm, the full output power corresponding to approximately 100 mW average power of the OPO was used to achieve the fluorescence image of N-GQD in the turbid tissue phantom with a quite high SNR.

Two-Photon Fluorescent Images of Cells at Different Z Positions

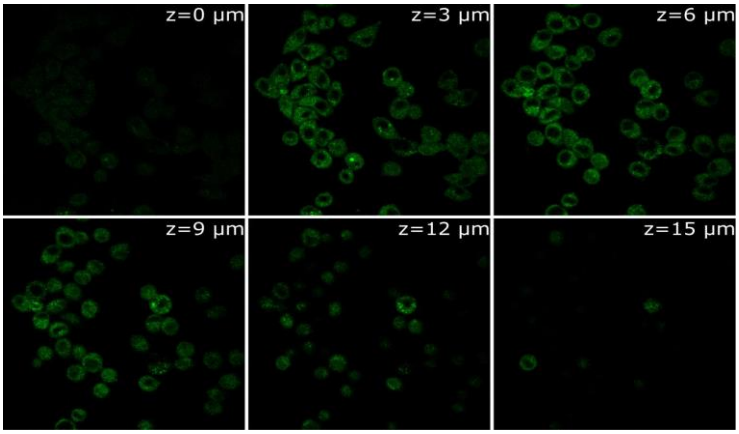

Figure:-6 Fluorescent images of cells incubated with N-GQDs at different Z positions (from the top 0 μm to the bottom 15 μm, Δz = 3 μm)

As the z axis moves from the top (0 μm) to the bottom (15 μm, Δz = 3μm), we can clearly observe the fluorescence spots throughout the z axis of the Hela cells. Therefore, it is safe to state that N-GQDs have been uptaken by cells and locate inside the cytoplasm rather than bounded or adsorbed on the surface of Hela cells.

Deep-Tissue Imaging Using the Monodispersed N-GQD Aqueous Solution

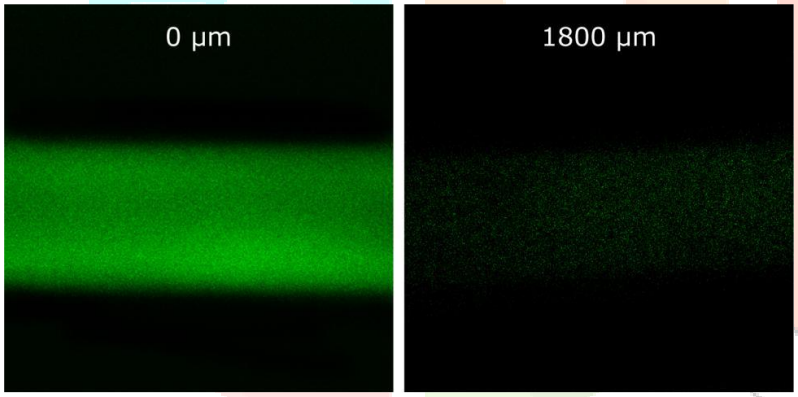

Figure:-7 Deep-tissue imaging using the monodispersed N-GQD solution loaded in a capillary

Deep-tissue imaging using the monodispersed N-GQD solution sample was also performed. We carefully used a capillary to load N-GQD aqueous solution. Then the capillary filled with N-GQD solution was placed in the tissue phantom for two-photon imaging. As shown in Figure 7 in the Supporting Information, the N-GQD solution sample could also emit bright fluorescence signal even in the deep tissue (~1800 μm). And the large two-photon absorption cross section and the high fluorescence QY could contribute to the bright fluorescence signal observed in the deep tissue. However, the focal plane was difficult to control at the same place of the capillary when we had to constantly adjust the capillary to locate at the different depth of the tissue phantom during the imaging experiment. So we used the dried N-GQD samples deposited on a cover slip which was marked with a red spot to help focusing on the same place of the cover slip at different imaging depths [93-97].

V. CELL GROWTH

Graphene oxide synthesis

Graphene oxide was synthesized from graphite using a simplified Hummers' method[98]. Graphite oxide was obtained by oxidation of 3 g of graphite flakes with 400 mL of H2SO4, and 18 g of KMnO4. The mixing process, using a magnetic stirrer, took less than 5 minutes to complete. However, to ensure complete oxidation of the graphite, the mixture was stirred for three days. During oxidation, the color of the mixture changed from dark purplish-green to dark brown. To stop the oxidation process, H2O2 solution was added and the color of the mixture changed to bright yellow, indicating a high oxidation level of graphite. The graphite oxide formed was washed three times with 1 M of aqueous HCl solution and repeatedly with deionized water until a pH of 4–5 was achieved. The washing process was carried out using a simple decantation of the supernatant with a centrifugation

technique. During the washing process with deionized water, the graphite oxide underwent exfoliation, which resulted in thickening of the graphene oxide solution, forming graphene oxide gel which was freeze-dried to obtain the graphene oxide solid.

Fabrication of graphene hydrogel

Graphene hydrogel was fabricated according to the method described by Xu et al with some modifications[98]. Ten milliliters of homogeneous graphene oxide aqueous dispersion at a concentration of 2 mg/mL, was sealed in a 16 mL Teflonlined autoclave and maintained at 180°C for 44 hours. The autoclave was allowed to cool to room temperature, and the fabricated graphene hydrogel was removed using tweezers and the surface adsorbed water was removed with filter paper. This sample was labeled graphene hydrogel (HG)-2. Graphene hydrogels at concentrations of 1.0, 0.5, and 0.1 mg/mL were also prepared using the same procedure, and were denoted as graphene HG-1, graphene HG-0.5, and graphene HG-0.1, respectively. To investigate the effect of the lateral dimension of graphene oxide, graphene oxide solution at a concentration at 2 mg/mL was sonicated for 1 hour before being processed using the procedure described above. This sample was labeled as graphene HGS-2

.

Characterization of graphene hydrogel

Measurement of the surface area of graphene hydrogel was done using a Micromeritics ASAP 2010 physisorption analyzer. The sample was placed into a sample tube, connected to the analyzer, and evacuated. Nitrogen BET surface area was calculated automatically by the system software. Field emission scanning electron microscopy images were obtained on a FEI Nova NanoSEM 400 operated at 10.0 kV. The crystalline phase was determined using a Phillips x-ray diffractometer employing a scanning rate of 0.033 degrees per second in a 2θ range from 5° to 80° with Cu Kα radiation (λ= 1.5418 Å). Chemical bonding was analyzed using a Perkin Elmer Fourier transform infrared spectroscope. The spectra (% transmittance with wave number) were recorded.

VI. CELL CULTURE

The graphene HG-2 sample was cut and placed into a 24-well plate. Each graphene hydrogel sample was seeded with 30,000 MG63 cells per well. Cells seeded directly on the 24-well plate served as the control. Prior to cell seeding on scaffolds, a cell count was performed using a Haemacytometer (Hirschmann Laborgerate), and 500 µL media with 10% heat-inactivated fetal bovine serum was added to each well for cell proliferation. MG63 cells were maintained using minimum essential medium supplemented with 10% heat-inactivated fetal bovine
serum, 1% penicillin/streptomycin, and 1 mM sodium pyruvate at 37°C in a humidified 5% CO2 atmosphere. Graphene hydrogel was incubated with the cells for one, three, five, and
seven days. The media were changed every three days.

MTT assay was used to determine the proliferation rate of MG63 on the graphene HG-2 scaffold. After each incubation period, MTT solution of 50 µL was added to each well and left for 4 hours for a cell response to take place. This was followed by addition of 500 µL of dimethyl sulfoxide to dissolve the purple crystals reduced by the living cells. The optical density, at 570 nm, of 200 µL of the resulting solution was measured using a spectrophotometer (Varioskan Flash, Finland).

VII. CELL MORPHOLOGY

Seeding by 30,000 MG63 cells was carried out on graphene hydrogel for morphological observation. Cells incubated on graphene hydrogel for days 1, 3, 5, and 7 were examined
using field emission scanning electron microscopy. Prior to viewing by field emission scanning electron microscopy, cells growing on the graphene hydrogel were washed with phosphate-buffered saline, and fixed with 4% of glutaraldehyde for 30 minutes at 4°C. Subsequently, the graphene hydrogel containing the cells was dehydrated through a series of graded alcohols and dried with hexamethyldisilazane at room temperature. The graphene hydrogel were then ready for observation by field emission scanning electron microscopy.

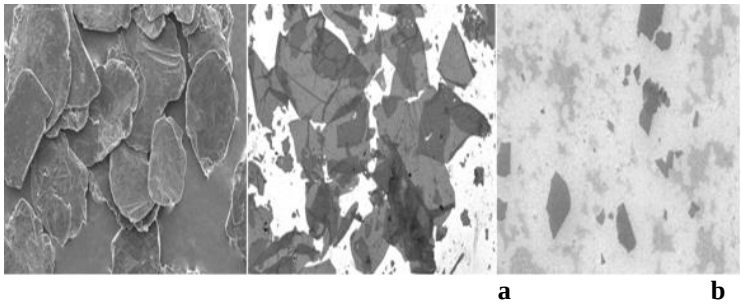

a b c

Figure:-8 Field emission scanning electron microscopy images of (a) graphite flakes, (b) large area graphene oxide sheets, and (c) sonicated graphene oxide sheets.

A simplified Hummers' method was used to produce largearea graphene oxide nanosheets. The large lateral dimension graphite flakes, which were used to produce the large-area graphene oxide, are shown in Figure 13a, and the resulting graphene oxide is shown in Figure 1b. The large graphene oxide has an average area of 7000 µm² and a lateral dimension

of up to 150 μm. After being sonicated for 1 hour, the average area is significantly reduced and the lateral dimension is reduced to <5 μm, as shown in Figure 13c [100].

Steam cell Differentiation

Human mesenchymal stem cells (hMSCs) are critical for numerous groundbreaking therapies in the field of regenerative medicine. A myriad of environmental factors including their interaction with soluble growth factors, extracellular matrices and neighboring cells are crucial for their survival, proliferation and differentiation into specific lineages[101-103]. One of the main goals of tissue engineering is to control these factors by creating physical and chemical microenvironments designed to guide the ultimate fate of stem cells. Materials with different elasticity, rigidity and texture have been extensively investigated for this purpose. Stem cell scaffolds, which can be both 2D and 3D in nature, have been fabricated to mimic the intrinsic characteristics of natural substrates such as muscle, bone and cartilage[104-106]. Recently, both the lithographic patterning of suitable surfaces such as polydimethylsiloxane (PDMS),[107] polymethyl methacrylate (PMMA),[108] self-assembled titanium dioxide (TiO2)[109] rod arrays and functionalized carbon nanotubes[110] have been explored. While there have been tremendous advances in this field, many challenges still remain. In particular in the field of bone tissue engineering, almost all artificial materials require the multiple administration of growth factors to promote hMSC differentiation. In addition, many approaches face challenges.

when it comes to scalability andcompatibility with implants. For example, an alloplastic (non-biologic) material under mechanical stress may not respond in a similar way as the surrounding host bone, resulting in structural failure of the implant or inflammatory changes in the original bone, as seen in stress shielding[111]. Also, bioactive implants still face limitations in terms of potential pathogenic infections, low availability and high costs. Graphene[112] may provide an elegant solution to some of these challenges. Being only one atom thick, it introduces the least amount of artificial material possible and has a large number of remarkable properties[113]. In the context of tissue engineering, its mechanical properties are likely to play a key role: graphene has the highest Young's modulus (0.5 – 1 TPa) among any known material, yet it is not brittle[114,115].Graphene can be transferred onto any flat or irregular shaped surface and graphene–coated, flexible, supporting substrates can be easily bent into any shape required[116].

Stem cell research with graphene has become feasible only with the recent availability of cheap, high quality, continuous graphene sheets on a large scale[117] Here we show that graphene provides a new type of biocompatible scaffold for stem cells. Remarkably, graphene accelerates cell differentiation even in the absence of commonly used additional growth factors such as BMP-2. Taking into consideration both the intrinsic mechanical properties of graphene and the striking results of this study, we envisage a functional role of this new material as a versatile platform for future biomedical applications in general and stem cell therapies in particular.

Large-scale graphene used in this study was synthesized by the chemical vapor deposition method on copper foils. After growth, copper was etched and the same batch of graphene was transferred to four distinct substrates used in this study according to methods discussed elsewhere[118]. We studied the influence of graphene on stem cell growth by investigating four substrates with widely varying stiffness and surface roughness: (1) polydimethylsiloxane (PDMS), (2) polyethylene terephthalate (PET), (3) glass slide and (4) silicon wafer with 300nm SiO2 (Si/SiO2) (Table S1 in Supporting Information). Plain cover slips without graphene were used as a control or reference for normalization. Atomic Force Microscopy (AFM) was used to analyze the surface roughness of the various substrates with and without graphene coating. Transferred to PET and PDMS, the graphene sheet exhibits nano-ripples with high density (Figure14c,d) compared to graphene on Si/SiO2 and glass slide (Figure 14a,b). Despite being only oneatom thick, on Si/SiO2 substrates with well-defined oxide thickness, graphene can be easily seen with a simple conventional optical microscope (Figure 9e). Therefore, detailed studies such as the evolution of cell differentiation with time were done mainly on graphene coated Si/SiO2 substrates. Two distinct sets of experiments were performed. First cell viability was studied with cells cultured in normal stem cell medium. Next, stem cell differentiation was examined in cells cultured on conventional osteogenic media

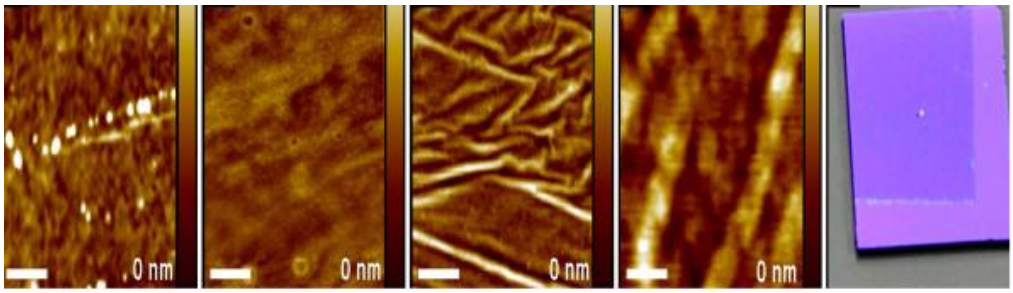

a b c d e

Figure: - 9 Graphene onto different substrates. AFM of graphene on (a) Si/SiO2 (b) Glass slide (c) PET-film and (d) PDMS. Scale bars are 200nm (e) Optical image of 1cm x 1cm, partially graphene coated Si/SiO2 chip, showing the graphene boundary.

Cell viability and morphology

The cell morphology and viability by image analysis on all four substrates with and without graphene coverage when cells were cultured in normal stem cell media. From Figure 10a we see that, independent of the substrate, there is no significant difference ($p>0.05$) in cell viability between graphene-coated and uncoated substrates. We also performed MTT assays (Fig. S2 in SI) to confirm the cell viability data. Again, regardless of the substrate, there was no difference ($p>0.05$) between uncoated and graphene-coated substrates, demonstrating that cell growth was indeed not affected by the presence of graphene. Note that cell viability is lower on PET and PDMS independent of the presence of graphene.

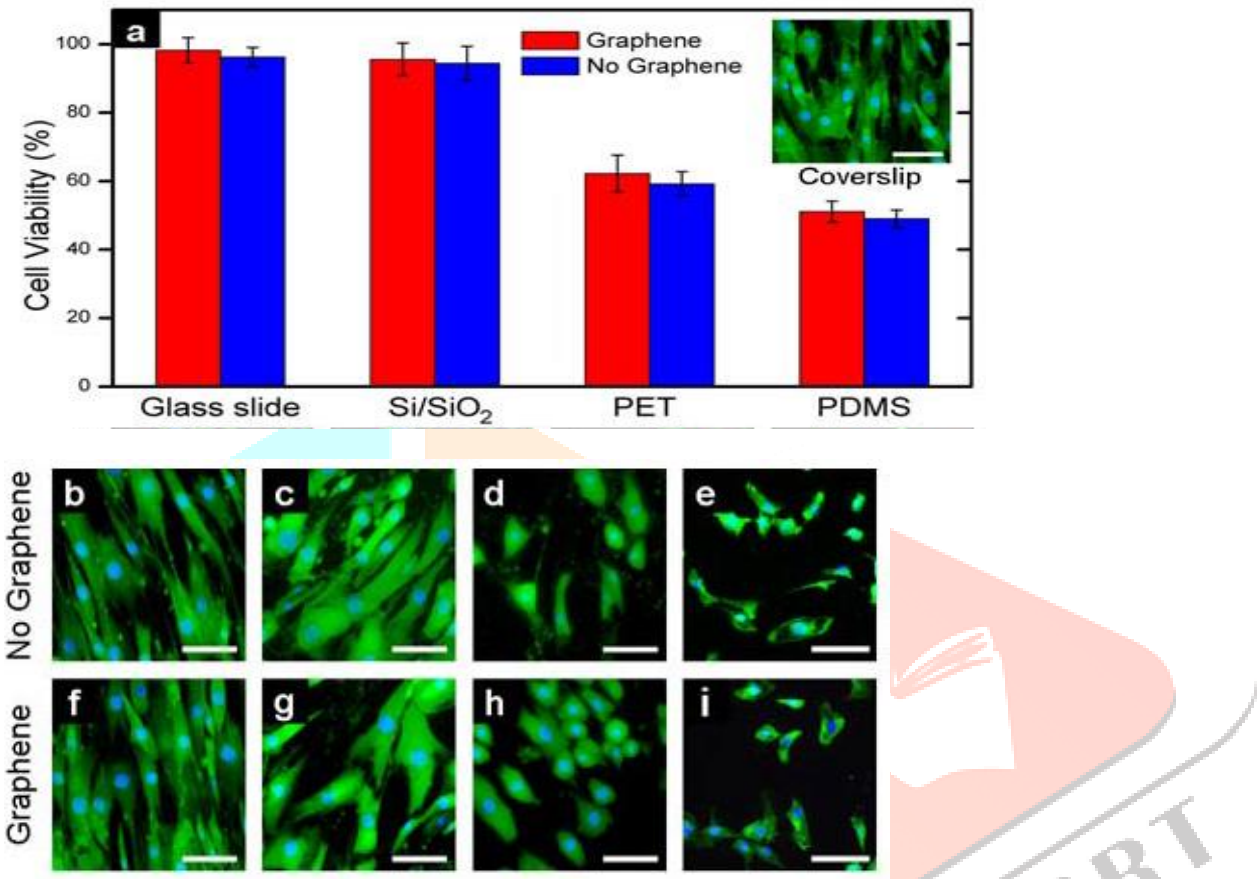

Figure:-10. Cell viability and morphology of hMSCs grown on different substrates. Cells are stained with DAPI (blue) and Calcein AM (green). (a) Graph showing cell viability in percentage normalized to cover slips used as reference. (Inset) Morphology of hMSCs grown on standard cover slips. (b-e) hMSCs grown on glass slide, Si/SiO2, PET and PDMS without graphene. (f-i) hMSCs grown on graphene coated glass slide, Si/SiO2, PET and PDMS. Scale bars are 100μm.

A similar conclusion can be reached by just comparing cell morphology with and without graphene. In general, the presence of graphene (Figure 10 f-i) did not influence the shape of the cells in comparison to uncoated substrates (Figure 10 b-e). Mesenchymal stem cells maintained their spindle-shape across glass A similar conclusion can be reached by just comparing cell morphology with and without graphene. In general, the presence of graphene (Figure 10 f-i) not influence the shape of the cells in comparison touncoated substrates (Figure 10b-e). Mesenchymal stem cells maintained their spindle-shape across glass 6 slides and Si/SiO2 after 15 days of incubation (Figure 10 b,c and Figure 10 f,g). Here stem cells presented the usual elongated structure with noticeable filopodia extensions and cellular propagation fronts. In the case of PET and PDMS, cells showed rounded or irregular morphology, most probably due to poor adhesion to the substrate (Figure 10 d,e and Figure 10 h,i). This suggests that graphene does not hamper the normal growth of stem cells and that the incorporation of this material in implants or injured tissues would not affect the physiological conditions of the microenvironment. In fact, Raman measurements and visual inspection of the samples after cell incubation and subsequent removal clearly.

Reference

[1] C.N.R. Rao, et al. Angew. Chem. Int. Ed. 48 (42) (2009) 7752.
[2] Y. Sun, et al. Energy Environ. Sci. 4 (4) (2011) 1113.
[3] N.G. Sahoo, et al. Adv. Mater. 24 (30) (2012) 4203.
[4] S. Zhang, et al. J. Mater. Chem. A 1 (15) (2013) 4631.
[5] Y. Shao, et al. Electroanalysis 22 (10) (2010) 1027.
[6] Y. Liu, et al. Chem. Soc. Rev. 41 (6) (2012) 2283.
[7] D. Chen, et al. Chem. Rev. 112 (11) (2012) 6027.
[8] J.H. Shen, et al. Chem. Commun. 48 (31) (2012) 3686.
[9] Y. Wang, et al. Trends Biotechnol. 29 (5) (2011) 205.
[10] P. Avouris, C. Dimitrakopoulos, Mater. Today 15 (3) (2012) 86.
[11] Z. Liu, et al. J. Am. Chem. Soc. 130 (33) (2008) 10876.
[12] Y. Zhu, et al. Adv. Mater. 22 (35) (2010) 3906.
[13] N.O. Weiss, et al. Adv. Mater. 24 (43) (2012) 5782.
[14] X. An, et al. ACS Nano 5 (2) (2011) 1003.
[15] A.A. Balandin, et al. Nano Lett. 8 (3) (2008) 902.
[16] V. Georgakilas, et al. Chem. Rev. 112 (11) (2012) 6156.
[17] X. Huang, et al. Chem. Soc. Rev. 41 (2) (2012) 666.
[18] K. Ostrikov, et al. Adv. Phys. 62 (2) (2013) 113–224.

[19] X. Sun, et al. Nano Res. 1 (3) (2008) 203.
[20] K. Yang, et al. Chem. Soc. Rev. 42 (2) (2013) 530.
[21] Y. Zhang, et al. Nanoscale 4 (13) (2012) 3833.
[22] H. Shen, et al. Theranostics 2 (3) (2012) 283.
[23] E. Morales-Narvaez, A. Merkoci, Adv. Mater. 24 (25) (2012) 3298.
[24] Z. Tang, et al. Small 6 (11) (2010) 1205.
[25] V. Georgakilas, Chem. Rev. 112 (11) (2012) 6156.
[26] J.T. Robinson, et al. J. Am. Chem. Soc. 133 (17) (2011) 6825.
[27] M. Li, et al. Adv. Mater. 24 (13) (2012) 1722.
[28] Avouris P, Dimitrakopoulos C: Graphene: synthesis and applications. Mater Today 2012, 15:86–97.
[29] Singh, V, Joung, D, Zhai, L, Das, S, Khondaker, S. I, & Seal, S. Graphene based materials: Past, present and future," Progress in Materials Science, (2011). , 56, 1178-1271.
[30] Zhu, Y, Murali, S, Cai, W, Li, X, Suk, J. W, Potts, J. R, & Ruoff, R. S. Graphene and Graphene Oxide: Synthesis, Properties, and Applications," Advanced Materials,(2010). , 22, 3906-3924.
[31] Mao, S, Pu, H, & Chen, J. Graphene oxide and its reduction: modeling and experimentalprogress," RSC Adv.,(2012). , 2, 2643-2662.
[32] Marcano, D. C, Kosynkin, D. V, Berlin, J. M, Sinitskii, A, Sun, Z, Slesarev, A, Alemany,
L. B, Lu, W, & Tour, J. M. Improved Synthesis of Graphene Oxide," ACS Nano, (2010). , 4, 4806-4814.
[33] Pei, S, & Cheng, H. -M. The reduction of graphene oxide," Carbon, (2012). , 50, 3210-3228.
[34] Chen, C, Yang, Q. -H, Yang, Y, Lv, W, Wen, Y, Hou, P. -X, Wang, M, & Cheng, H. -M. Self-Assembled Free-Standing Graphite Oxide Membrane," Adv. Mater., (2009). , 21,3007-3011. Graphene Oxide Based Surface Plasmon Resonance Biosensors http://dx.doi.org/10.5772/56221 211
[35] Bai, S, & Shen, X. Graphene-inorganic nanocomposites," RSC Advances, (2012). , 2,64-98.
[36] Guo, Y, Di, C. -A, Liu, H, Zheng, J, Zhang, L, Yu, G, & Liu, Y. General route toward patterning of graphene oxide by a combination of wettability modulation and spincoating,"ACS Nano (2010). , 4, 5749.
[37] Dong, X, Huang, W, & Chen, P. In Situ Synthesis of Reduced Graphene Oxide and Gold Nanocomposites for Nanoelectronics and Biosensing," anoscale Res Lett., (2011). , 6, 1-6.
[38] Fu, W. Y, Liu, L, Wang, W. L, Wu, M. H, Xu, Z, Bai, X. D, & Wang, E. G. Carbon nanotube transistors with graphene oxide films as gate dielectrics," Science China: Physics, Mechanics and Astronomy, (2010). , 53, 828-833.
[39] Loh, K. P, Bao, Q, Eda, G, & Chhowalla, M. Graphene oxide as a chemically tunable platform for optical applications," Nature Chemistry, (2010). , 2, 1015-1024.
[40] Dreyer, D. R, Park, S, Bielawski, C. W, & Ruoff, R. S. The chemistry of graphene oxide," Chem.Soc.Rev.,(2010). , 39, 228-240.
[41] Lim, G. -K, Chen, Z. -L, Clark, J, Goh, R. G. S, Ng, W. -H, Tan, H. -W, Friend, R. H, Ho, P. K. H, & Chua, L. -L. Giant broadband nonlinear optical absorption response in dispersed graphene single sheets," Nature Photonics, (2011). , 5, 554-560.
[42] Shukla, S, & Saxena, S. Spectroscopic investigation of confinement effects on optical
properties of graphene oxide" Appl. Phys. Lett. 98, 073104, (2011).
[43] Johari, P, & Shenoy, V. B. Modulating Optical Properties of Graphene Oxide: Role ofProminent Functional Groups," ACS Nano,(2011). , 5, 7640-7647.
[44] Bao, Q, & Loh, K. P. Graphene Photonics, Plasmonics, and Broadband OptoelectronicDevices," ACS Nano, (2012). , 6, 3677-3694.
[45] Chiu, N. -F, Huang, T. -Y, Kuo, C. -C, Lee, W. -C, Hsieh, M. -H, & Lai, H. -C. Single- Layer Graphene based SPR biochips for tuberculosis bacillus detection," Proc. ofSPIE (2012). , 8427, 84273M1-84273M7.
[46] Liu, Y, Dong, X, & Chen, P. Biological and chemical sensors based on graphene materials," Chem. Soc. Rev., (2012). , 41, 2283-2307.
[47] Dong, X, Long, Q, Wang, J, Chan-park, M. B, Huang, b, Y, Huang, W, & Chen, P. A graphene nanoribbon network and its biosensing application," Nanoscale, (2011). , 3,5156-5160.

[48] Morales-narváez, E, & Merkoçi, A. Graphene Oxide as an Optical Biosensing Platform," Adv. Mater., (2012). , 24, 3298-3308.
[49] Chen, D, Feng, H, & Li, J. Graphene Oxide: Preparation, Functionalization, and Electrochemical Applications" Chem. Rev., (2012). , 112, 6027. 212 Advances in Graphene Science
[50] Zhang, Y, Tan, Y. W, Stormer, H. L, & Kim, P. Experimental Observation of QuantumHall Effect and Berry's Phase in Graphene, Nature" (2005). , 438, 201-204.
[51] Loh, K. P, Bao, Q. L, Ang, P. K, & Yang, J. X. The chemistry of graphene," J. Mater. Chem., (2010). , 20, 2277-2289.
[52] Graphene oxide-based SPR biosensor chip for immunoassay applications Nan-Fu Chiu, Teng-Yi Huang, Hsin-Chih Lai and Kou-Chen Liu Chiu et al. Nanoscale Research Letters 2014, 9:445.
[53] Graphene Oxide Based Surface Plasmon Resonance Biosensors Nan-Fu Chiu, Teng-Yi Huang and Hsin-Chih Lai Additional information is available at the end of the chapter http://dx.doi.org/10.5772/56221.
[54] Y. Ohno, K. Maehashi, and K. Matsumoto, "Chemical and biological sensing applications based on graphene field-effect transistors," Biosensors & bioelectronics 26 (4), 1727-1730 (2010).
[55] Y. Ohno, K. Maehashi, Y. Yamashiro, and K. Matsumoto, "Electrolyte-gated graphene field-effect transistors for detecting pH and protein adsorption," Nano Lett 9 (9), 3318-3322 (2009).
[56] Y. Huang, X. Dong, Y. Shi, C. M. Li, L. J. Li, and P. Chen, "Nanoelectronic biosensors based on CVD grown graphene," Nanoscale 2 (8), 1485-1488 (2010).
[57] X. Dong, Y. Shi, W. Huang, P. Chen, and L. J. Li, "Electrical detection of DNA hybridization with single-base specificity using transistors based on CVD-grown graphene sheets," Adv Mater 22 (14), 1649-1653 (2010).
[58] Sudip Chakraborty and C. Retna Raj, "Amperometric biosensing of glutamate using carbon nanotube based electrode," Electrochemistry Communications 9 (6), 1323-1330 (2007).
[59] X. Kang, J. Wang, H. Wu, I. A. Aksay, J. Liu, and Y. Lin, "Glucose oxidasegraphene-
chitosan modified electrode for direct electrochemistry and glucose sensing," Biosensors & bioelectronics 25 (4), 901-905 (2009).
[60] U. Yogeswaran and S. M. Chen, "A review on the electrochemical sensors and biosensors composed of nanowires as sensing material," Sensors-Basel 8 (1), 290- 313 (2008).

[61] L. Tang, Y. Zhu, L. Xu, X. Yang, and C. Li, "Amperometric glutamate biosensor based on self-assembling glutamate dehydrogenase and dendrimer-encapsulated platinum nanoparticles onto carbon nanotubes," Talanta 73 (3), 438-443 (2007).
[62] R. C. Becker and F. A. Spencer, "Thrombin: Structure, Biochemistry, Measurement, and Status in Clinical Medicine," J Thromb Thrombolysis 5 (3), 215-229 (1998).
[63] M. L. Nierodzik and S. Karpatkin, "Thrombin induces tumor growth, metastasis, and angiogenesis: Evidence for a thrombin-regulated dormant tumor phenotype," Cancer cell 10 (5), 355-362 (2006).
[64] Steven R. Garden, George J. Doellgast, Kenneth S. Killham, and Norval J. C. Strachan, "A fluorescent coagulation assay for thrombin using a fibre optic evanescent wave sensor," Biosensors and Bioelectronics 19 (7), 737-740 (2004); Radislav A. Potyrailo, Richard C. Conrad, Andrew D. Ellington, and Gary M. Hieftje, "Adapting Selected Nucleic Acid Ligands (Aptamers) to Biosensors," Analytical Chemistry 70 (16), 3419-3425 (1998); C. H. Tung, R. E. Gerszten, F. A. Jaffer, and R. Weissleder, "A novel near-infrared fluorescence sensor for detection of thrombin activation in blood," Chem Bio Chem 3 (2-3), 207- 211 (2002).
[65] Y. Wu, Y. M. Lin, A. A. Bol, K. A. Jenkins, F. Xia, D. B. Farmer, Y. Zhu, and P. Avouris, "High-frequency, scaled graphene transistors on diamond-like carbon," Nature 472 (7341), 74-78 (2011).
[66] Longhua Tang Haixin Chang, Ying Wang, Jianhui Jiang, Jinghong Li, "Graphene Fluorescence Resonance Energy Transfer Aptasensor for the Thrombin Detection," Analytical Chemistry 82 (6), 2341-2346 (2010).
[67] Y. Ohno, K. Maehashi, and K. Matsumoto, "Label-Free Biosensors Based on Aptamer-Modified Graphene Field-Effect Transistors," Journal of the American Chemical Society 132 (51), 18012-18013 (2010).
[68] Baker, S. N. Baker, G. A. Angew. Chem., Int. Ed. 2010, 49, 6726−6744.
[69] Sun, X. M. Liu, Z. Welsher, K. Robinson, J. T. Goodwin, A. Zaric, S. Dai, H. J. Nano Res. 2008, 1, 203−212.
[70] Li, Q. Ohulchanskyy, T. Y. Liu, R. Koynov, K. Wu, D. Best, A. Kumar, R. Bonoiu, A. Prasad, P. N. J. Phys. Chem. C 2010, 114, 12062−12068.
[71] Pan, D. Y. Zhang, J. C. Li, Z. Wu, M. H. Adv. Mater. 2010, 22, 734−738.
[72] Peng, J. Gao, W. Gupta, B. K. Liu, Z. Romero, R. Ge, L. H. Song, L. Alemany, L. B. Zhan, X. B. Gao, G. H.; Vithayathil, S. A.
Kaipparettu, B. A. Marti, A. A. Hayashi, T. Zhu, J. J. Ajayan, P. M. Nano Lett. 2011, 12, 884−849.
[73] Cao, L. Wang, X. Meziani, M. J. Lu, F. Wang, H. F. Luo, P. G.; Lin, Y. Harruff, B. A.; Veca, L. M.; Murray, D. Xie, S. Y. Sun, Y.
P. J. Am. Chem. Soc. 2007, 129, 11318−11319.
[74] Li, J. L. Bao, H. C. Hou, X. L. Sun, L. Wang, X. G. Gu, M. Angew. Chem., Int. Ed. 2012, 51, 1830−1834.
[75] Qian, J. Wang, D. Cai, F. H.; Xi, W. Peng, L. Zhu, Z. F. He, H. Hu, M. L. He, S. Angew. Chem., Int. Ed. 2012, 51, 10570−10575.
[76] Zhu, S. Zhang, J. Tang, S. Qiao, C. Wang, L. Wang, H. Liu, X. Li, B. Li, Y. Yu, W. Wang, X. Sun, H. Yang, B. Adv. Funct. Mater. 2012, 22, 4732−4740.
[77] Li, Y. Zhao, Y.; Cheng, H. H. Hu, Y. Shi, G. Q. Dai, L. M. Qu, L. T. J. Am. Chem. Soc. 2012, 134, 15−18.
[78] Guo, B. D. Liu, Q. Chen, E. D. Zhu, H. W. Fang, L. Gong, J. R. Nano Lett. 2010, 10, 4975−4980.
[79] Guo, B. D. Fang, L. Zhang, B. H. Gong, J. R. Electron. Lett. 2011, 47, 663−664.
[80] Guo, B. D. Fang, L. Zhang, B. H. Gong, J. R. Insci. J. 2011, 1, 80−89.
[81] Li, Q. Zhang, S. Dai, L. Li, L. S. J. Am. Chem. Soc. 2012, 134, 18932−18935.
[82] Tetsuka, H. Asahi, R. Nagoya, A.; Okamoto, K. Tajima, I. Ohta, R. Okamoto, A. Adv. Mater. 2012, 24, 5333−5338.
[83] Ponomarenko, L. Schedin, F. Katsnelson, M. Yang, R. Hill, E. Novoselov, K. Geim, A. Science 2008, 320, 356−358.
[84] Girit, Ç. Ö. Meyer, J. C. Erni, R. Rossell, M. D. Kisielowski, C. Yang, L. Park, C. H. Crommie, M. Cohen, M. L. Louie, S. G. Science 2009, 323, 1705−1708.

[85] Loh, K. P. Bao, Q. L. Eda, G. Chhowalla, M. Nat. Chem. 2010, 2, 1015−1024.
[86] Padilha, L. A. Nootz, G. Olszak, P. D. Webster, S. Hagan, D. J. Van Stryland, E. W. Levina, L. Sukhovatkin, V. Brzozowski, L.
Sargent, E. H. Nano Lett. 2011, 11, 1227−1231.
[87] Luo, Z. T. Vora, P. M. Mele, E. J. Johnson, A. T. C. Kikkawa, J. M. Appl. Phys. Lett. 2009, 94, 111909−3.
[88] Trauzettel, B. Bulaev, D. V. Loss, D.;Burkard, G. Nat. Phys. 2007, 3, 192−196.
[89] Xu, Y. Bai, H. Lu, G. Li, C. Shi, G. J. Am. Chem. Soc. 2008, 130, 5856−5857.
[90] Tuinstra, F. Koenig, J. L. J. Chem. Phys. 1970, 53, 1126−1130.
[91] Ai, K. L.; Liu, Y. L.; Lu, L. H.; Cheng, X. L.; Huo, L. H. J. Mater. Chem. 2011, 21, 3365−3370.
[92] Mei, Q. S. Zhang, K.; Guan, G. J. Liu, B. H. Wang, S. H.Zhang, Z. P. Chem. Commun. 2010, 46, 7319−7321.
[93] Porres, L.; Holland, A.; Pålsson, L.O.; Monkman, A. P.; Kemp, C.; Beeby, A. J. Fluoresc. 2006, 16, 267.
[94] Compton, O. C.; Dikin, D. A.; Putz, K. W.; Brinson,L. C.; Nguyen, S. T. Adv. Mater. 2010, 22, 892.
[95] Li, Q.Gu o, B.; Yu, J. Ran, J.; Zhang, B. Yan, H. J.; Gong, J. R. J. Am. Chem. Soc. 2011. 133, 10878.
[96] Mei, Q.; Zhang, K.; Guan, G.; Liu, B.; Wang, S.; Zhang, Z. Chem. Comm. 2010, 46, 7319.
[97] Strong Two-Photon-Induced Fluorescence from Photostable, Biocompatible Nitrogen-Doped Graphene Quantum Dots for Cellular and Deep-Tissue Imaging Qian Liu, Beidou Guo, Ziyu Rao, Baohong Zhang, Jian Ru Gong*
National Center for Nanoscience and Technology, 11 Zhongguancun Beiyitiao, Beijing 100190, China.
[198] Hummers WS, Offeman RE. Preparation of graphitic oxide. J Am Chem Soc. 1958; 80:1339.
[99] Xu Y, Sheng K, Li C, Shi G. Self assembled graphene hydrogel via a one-step hydrothermal process. ACS Nano. 2010; 4:4324–4330.
[100] HN Lim,NM Huang,SS Lim,I Harrison,CH Chia Fabrication and characterization of graphene hydrogel via hydrothermal approach as a scaffold for preliminary study of cell growth International Journal of Nanomedicine 29aug 2011.
[101] Spradling, A. Drummond-Barbosa, D. Kai, T. Stem cells find their niche. Nature 2001, 414, 98–104.
[102] Lutolf, M. P. Hubbell, J. A. Synthetic Biomaterials as Instructive Extracellular Microenvironments for Morphogenesis in Tissue Engineering. Nature Biotechnol. 2005, 23, 47–55.
[103]Discher, D. E. Mooney, D. J. Zandstra, P. W. Growth Factors, Matrices, and Forces Combine and Control Stem Cells. Science 2009, 324, 1673–1677.
[104] Jaiswal, N. Haynesworth, S. E. Caplan, A. I. Bruder, S. P. Osteogenic Differentiation of Purified, Culture-Expanded Human Mesenchymal Stem Cells in Vitro. J. Cell Biochem. 1997, 64, 295–312.
[105] Engler, A. J. Sen, S. Sweeney, H. L.;Discher, D. E. Matrix Elasticity Directs Stem Cell Lineage Specification. Cell 2006, 126, 677–689.
[106] Reilly, G. C. Engler, A. J. Intrinsic Extracellular Matrix Properties Regulate Stem Cell Differentiation. J. Biomech. 2010, 43, 55–62.

[107]Kim, S. J. Lee, J. K.; Kim, J. W. Jung, J. W. Seo, K. Park, S. B. Roh, K. H.; Lee, S. R.Hong, Y. H. Kim, S. J. et al. Surface Modification of Polydimethylsiloxane (PDMS) Induced Proliferation and Neural-Like Cells Differentiation of Umbilical Cord Blood-Derived Mesenchymal Stem Cells. J. Mater. Sci: Mater. Med. 2008, 19, 2953–2962.
[108]Dalby, M. J. Gadegaard, N.; Tare, R. Andar, A. Riehle, M. O.; Herzyk, P. Wilkinson, C. D. W. Oreffo, R. O. C. The Control of Human Mesenchymal Cell Differentiation Using Nanoscale Symmetry and Disorder. Nat. Mater. 2007, 6, 997–1003.
[109] Oh, S. Brammer, K. S. Li, Y. S. J. Teng, D.; Engler, A. J. Chien, S. Jin, S. Stem Cell Fate Dictated Solely by Altered Nanotube Dimension. Proc. Natl. Acad. Sci. USA 2009, 106, 2130– 2135. 20
[110]Nayak, T. R. Jian, L. Phua, L. C. H o, H. K. Ren, Y. Pastorin, G. Thin Films of Functionalized Multiwalled Carbon Nanotubes as Suitable Scaffold Materials for Stem Cells
Proliferation and Bone Formation. ACS Nano, 2010, 4, 7717–7725.
[112] Konttinen, Y. T. Zhao, D. Beklen, A. Ma, G. Takagi, M. Kivelä-Rajamäki, M. Ashammakhi, N. Santavirta, S. The Microenvironment around Total Hip Replacement Prostheses. Clin. Orthop. Relat. Res. 2005, 430, 28–38.
[112] Novoselov, K. S. Geim, A. K. Morozov, S. V. Jiang, D. Zhang, Y.; Dubonos, S. V.
Grigorieva, I. V. Firsov, A. A. Electric Field Effect in Atomically Thin Carbon Films. Science 2004, 306, 666–669.
[113] A. K. Geim, Graphene: Status and Prospects. Science 2009, 324, 1530–1534.
[114] Frank, I. W.; Tanenbaum, D. M.; van der Zande, A. M.; McEuen, P. L. Mechanical Properties of Suspended Graphene Sheets. J. Vac. Sci. Technol. B 2007, 25, 2558–2561.
[115] Lee, C. Wei, X. Kysar, J. W. Hone, J. Measurement of the Elastic Properties and Intrinsic Strength of Monolayer Graphene. Science 2008, 321, 385–388.
[116] Lee, Y. Bae, S. Jang, H. Jang, S. Zhu, S.-E. Sim, S. H. Song, Y. I. Hong, B. H. Ahn, J.- H. Wafer-Scale Synthesis and Transfer of Graphene Films. Nano Lett. 2010, 10, 490–493.
[117] Bae, S. Kim, H. Lee, Y. Xu, X. Park, J.
S. Zheng, Y. Balakrishnan, J.; Lei, T. Kim, H. R. Song, Y. I. et al. Roll-to-Roll Production of 30-Inch Graphene Films for Transparent
Electrodes. Nat. Nano, 2010, 5, 574–578.
[118] Li, X. Cai, W. An, J. Kim, S. Nah, J. Yang, D. Piner, R. Velamakanni, A. Jung, I. Tutuc, E. et al. Large-Area Synthesis of High-Quality and Uniform Graphene Films on Copper Foils. Science 2009, 324, 1312–1314.